Tumor Imaging

DOI: 10.1002/ange.201408442

Targeted Imaging and Proteomic Analysis of Tumor-Associated Glycans in Living Animals**

*Ran Xie, Lu Dong, Rongbing Huang, Senlian Hong, Ruoxing Lei, and Xing Chen**

Abstract: *Although it has been well known that dynamic changes in glycosylation are associated with tumor progression, it remains challenging to selectively visualize the cancer glycome in vivo. Herein, a strategy for the targeted imaging of tumor-associated glycans by using ligand-targeted liposomes encapsulating azidosugars is described. The intravenously injected liposomal nanoparticles selectively bound to the cancer-cell-specific receptors and installed azides into the melanoma glycans in a xenograft mouse model in a tissue-specific manner. Subsequently, a copper-free click reaction was performed in vivo to chemoselectively conjugate the azides with a near-infrared fluorescent dye. The glycosylation dynamics during tumor growth were monitored by in vivo fluorescence imaging. Furthermore, the newly synthesized sialylated glycoproteins were enriched during tumor growth and identified by glycoproteomics. Compared with the labeling methods using free azidosugars, this method offers improved labeling efficiency and high specificity and should facilitate the elucidation of the functional role of glycans in cancer biology.*

The green fluorescent protein (GFP) and its variants have revolutionized the molecular imaging of proteins.[1] Proteins of interest can be genetically fused with GFP and visualized in live cells and living animals. This strategy, however, cannot be directly extended to study other biomolecules such as glycans, as they are not genetically encoded. Alternatively, glycans can be metabolically labeled with azidosugars, followed by covalent conjugation with fluorescent probes by bioorthogonal chemistry.[2,3] This metabolic glycan labeling technique has greatly compensated for the lack of methods available for glycan imaging that are analogous to GFP. However, unlike GFP fusions, which can be conveniently targeted to specific tissues by employing the proper tissue-specific promoters,[3–5] the metabolic glycan labeling technique cannot selectively label glycans in a specific tissue of interest in vivo. Upon administration to mice, azidosugars are metabolized and incorporated into glycans in various tissues.[6–8] The lack of tissue selectivity has limited the use of azidosugars for in vivo glycan imaging where probing glycosylation in a specific tissue is desired, for example, the targeted imaging of tumor-associated glycans.

Herein, we describe the realization of selective labeling and targeted imaging of glycans in a tissue-selective manner in vivo using ligand-targeted liposomes encapsulating azidosugars (Figure 1). Accumulating evidence has indicated that altered cell surface glycosylation accompanies tumor progression at various pathophysiological stages.[9,10] We therefore chose to demonstrate our strategy by targeted labeling and imaging of tumor-associated glycans in vivo. We have previously developed ligand-targeted liposomes encapsulating azidosugars for selectively labeling glycans of specific cell types in cell cultures.[11] We envisioned that the liposomal azidosugar-based strategy could be extended for tumor-targeted glycan labeling in vivo. In particular, sialic acids, which are often the terminal monosaccharides of cell-surface glycans, have been shown to play an important role in tumor growth and metastasis.[12–14] Several sialylated glycans, including sialyl Lewis X[15] and sialyl Tn,[16] have been identified as

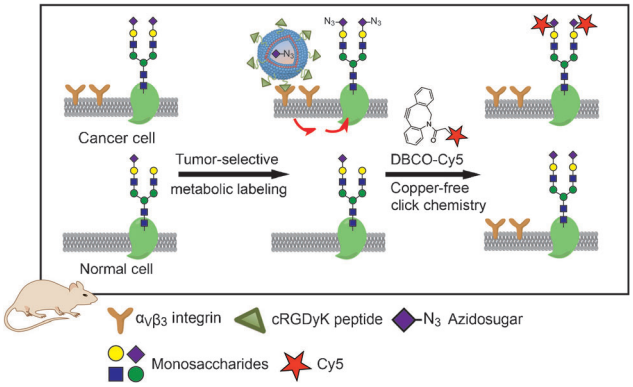

Figure 1. Targeted imaging of the cancer glycome in vivo. The ligand-targeted liposomes encapsulating azidosugars are intravenously injected into the tumor-bearing mice. The ligands (e.g., cRGDyK) are selectively recognized by the cell-surface receptors (e.g., $\alpha_v\beta_3$) expressed on the tumors, which induces the internalization of the liposomal azidosugars into the cancer cells. The azidosugars are utilized by biosynthetic enzymes and incorporated selectively into tumor-associated glycans, and then directly visualized by copper-free click chemistry in vivo.

[*] R. Xie, L. Dong, R. Huang, S. Hong, R. Lei, Prof. X. Chen
Beijing National Laboratory for Molecular Sciences
Key Laboratory of Bioorganic Chemistry and Molecular Engineering of Ministry of Education
College of Chemistry and Molecular Engineering
Synthetic and Functional Biomolecules Center
Peking–Tsinghua Center for Life Sciences
Peking University, Beijing 100871 (P.R. China)
E-mail: xingchen@pku.edu.cn

[**] We thank Dr. R. Meng in the mass spectrometry facility of the National Center for Protein Sciences at Peking University for assistance with proteomic analysis, and H. He and Y. Li for assistance with animal experiments. This work was supported by the National Basic Research Program of China (973 Program; 2012CB917303) and the National Natural Science Foundation of China (21172013, 91127034, and 91313301)

Supporting information for this article is available on the WWW under http://dx.doi.org/10.1002/anie.201408442.

tumor-associated antigens. We therefore chose to evaluate our liposomal azidosugar-based method by probing sialylated glycans in a xenograft model of melanoma in living mice.

Before performing in vivo experiments, we confirmed the selectivity in B16–F10 cells, a mouse melanoma cell line, which exhibit sialic acid-correlated high metastatic potential.[17,18] We employed a cyclic Arg–Gly–Asp–D-Tyr–Lys (cRGDyK) pentapeptide as the targeting ligand.[19,20] The RGD-containing peptide is recognized by integrin $\alpha_V\beta_3$, which is overexpressed on the B16–F10 cell surface.[21,22] To prepare $\alpha_V\beta_3$-targeting liposomes, we conjugated cRGDyK to an *N*-hydroxylsuccinamide (NHS)-activated PEGylated distearoylphosphatidylethanolamine (DSPE), DSPE–PEG2000–NHS. The resulting RGD-containing lipid, DSPE–PEG2000–cRGDyK, together with dioleoylphosphatidylcholine (DOPC) and cholesterol at a molar ratio of 50:50:5, was used to fabricate the cRGDyK-functionalized and PEGylated liposome (cRGD–LP) with a diameter of approximately 200 nm. 9-Azido sialic acid (9AzSia) was encapsulated at an azidosugar to lipid molar ratio of approximately 1.2:1 to obtain cRGD–LP–9AzSia for the targeted labeling of sialylated glycans in B16–F10 cells (Supporting Information, Table S1). MCF-7 cells with a low expression level of integrin $\alpha_V\beta_3$ were used as a negative control. The cells were incubated with cRGD–LP–9AzSia (10–100 μM, calculated based on the 9AzSia concentration) for 24 hours, followed by reaction with the aza-dibenzocyclooctyne–Cy5 conjugate (DBCO–Cy5) through copper-free click chemistry.[23,24] Confocal fluorescence microscopy and flow cytometry showed significant labeling of cell-surface sialylglycoconjugates in B16–F10 cells and much lower labeling in MCF-7 cells (Figure S1). When the cells were treated with 9AzSia encapsulated in liposomes without the cRGDyK ligand (LP–9AzSia), the cell-selective labeling was diminished. These results indicate that cRGD–LP–9AzSia selectively labels the sialylated glycans on the targeted B16–F10 cells, prompting us to evaluate the in vivo targeting efficacy.

To evaluate cRGD–LP–9AzSia in vivo, we tested the targeted glycan labeling in a melanoma xenograft mouse model. B16–F10 cells were implanted into one side of the flank of Balb/c mice, and MCF-7 cells were implanted into the other side as a control tumor that is not targeted by cRGD–LP–9AzSia. The two types of tumors exhibited a similar growth rate (Figure S2a). The administration of liposomal azidosugars did not affect the tumor growth rates (Figure S2b,c). Furthermore, we evaluated the circulation time of the near-infrared dye DBCO–Cy5 and determined that it had mostly been cleared from the blood stream of the mice with no cRGD–LP–9AzSia administration after three hours, leaving minimal background fluorescence (Figure S3a). The tumor-bearing mice were then intravenously injected daily with cRGD–LP–9AzSia (235 mg kg^{-1}, calculated based on 9AzSia) for seven days. On the eighth day, DBCO–Cy5 (0.14 nmol kg^{-1}) was injected into the tail vein. After the copper-free click reaction had occurred inside the living animals and the excess DBCO-Cy5 had been cleared from the bloodstream in five hours, the mice were subjected to whole-body fluorescence imaging. We observed strong fluorescence on the melanoma xenograft, corresponding to the cell-surface sialylglycoconjugates (Figure 2a). The tumor-to-background ratio (TBR) was quantified to be 177.0 ± 16.8 (mean ± s.d.). Importantly, the xenograft of the MCF-7 tumor in the same mouse exhibited minimal fluorescence, and a positive-to-negative tumor ratio (PNR) of 5.9 ± 0.3 was achieved (Figure 2f). Time course fluorescence imaging of the labeled mice confirmed that the excess free DBCO–Cy5 had been cleared three hours after injection, and the dyes chemically conjugated onto the 9AzSia-incorporated tumor-associated glycans remained detectable for up to 24 hours (Figure S3b). Notably, strong labeling was also observed in several organs, including the kidney, liver, and spleen (Figure 2a), which was

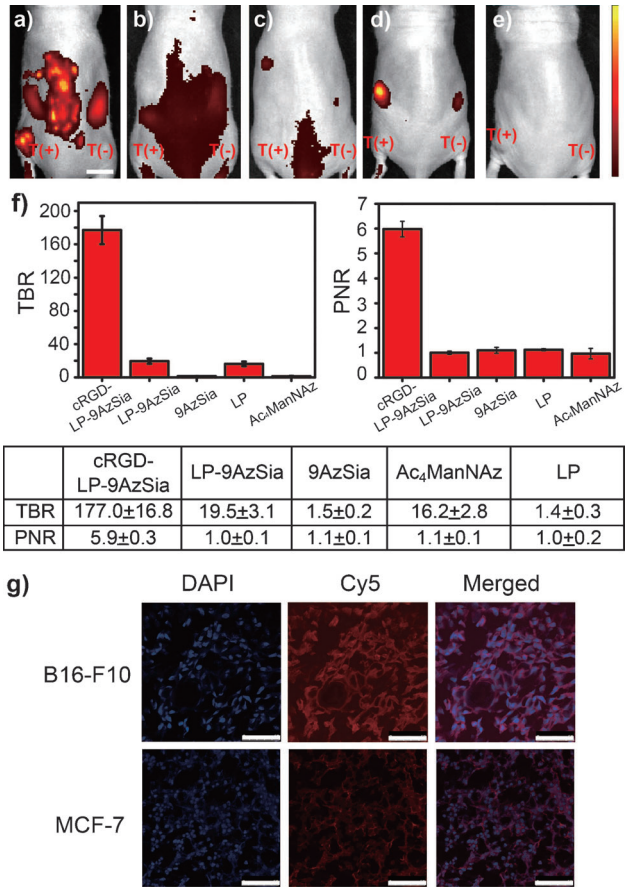

	cRGD-LP-9AzSia	LP-9AzSia	9AzSia	Ac_4ManNAz	LP
TBR	177.0±16.8	19.5±3.1	1.5±0.2	16.2±2.8	1.4±0.3
PNR	5.9±0.3	1.0±0.1	1.1±0.1	1.1±0.1	1.0±0.2

Figure 2. Targeted in vivo imaging of tumor-associated sialylated glycans using cRGD–LP–9AzSia. a–e) Whole-body fluorescence images of tumor-bearing mice administered with cRGD–LP–9AzSia (235 mg kg^{-1}; a), LP-9AzSia (235 mg kg^{-1}; b), 9AzSia (235 mg kg^{-1}; c), Ac_4ManNAz (300 mg kg^{-1}, equimolar to 9AzSia; d), and LP (e) for 7 days. DBCO–Cy5 was then injected into the mice. Shown are representative ($n = 5$ mice per group) images at 5 h after dye injection. T(+) = integrin $\alpha_v\beta_3$-positive B16–F10 tumor, T(−) = integrin $\alpha_v\beta_3$-negative MCF-7 tumor. The color-coded scale is for the fluorescence intensity. Scale bar: 1 cm. f) Quantification of the fluorescence signal. TBR: The contrast-to-background ratio (CBR) of the tumor divided by the CBR of nearby normal tissue. PNR: The CBR of a B16–F10 tumor divided by the CBR of an MCF-7 tumor. All fluorescence images were taken using the same exposure time. Error bars represent the standard deviation from five experiments. g) Fluorescence images of tumor tissue sections from mice treated with cRGD–LP–9AzSia. The nuclei were visualized by staining with 4′,6-diamidino-2-phenylindole (DAPI; blue signal). Scale bars: 100 μm.

probably due to renal clearance, as well as accumulation of cRGD–LP–9AzSia in the liver and spleen, as confirmed by ex vivo imaging of the isolated organs (Figure S4). We also isolated the tumor tissues and performed high-resolution fluorescence imaging on the tissue sections (Figure 2g). A much higher fluorescence intensity was observed in the B16–F10 tumor sections, in agreement with the in vivo imaging experiments. These results suggest that the targeted labeling of sialylated glycans on the $\alpha_V\beta_3$-positive tumors using cRGD–LP–9AzSia is achieved by an active targeting mechanism that is based on specific ligand–receptor interactions.

Tumors may also be passively targeted by accumulating liposomes or other nanocarriers in tumors by the enhanced permeability and retention (EPR) effect.[25,26] As a comparative study, we injected LP–9AzSia into the tumor-bearing mice. Much lower labeling was observed for the tumor tissues (Figure 2b; see also Figure S5). TBR and PNR were quantified as 19.5 ± 3.1 and 1.0 ± 0.1, respectively (Figure 2f). These results suggest that the EPR effect alone is not sufficient for the selective labeling of tumor-associated glycans by liposomal azidosugars at the designated dosages. Rather, active ligand targeting is essential in our system.

We also evaluated the targeting efficiency of the free azidosugars. 9AzSia, at the dosages giving an equal amount of azidosugars as the cRGD–LP–9AzSia administration, was intravenously injected into the tumor-bearing mice and labeled with DBCO–Cy5. As expected, a low-intensity fluorescence signal was observed for the tumor tissues (Figure 2c; see also Figure S5). Furthermore, we tested Ac_4ManNAz by intraperitoneal injection, using dosages similar to those previously used to label sialylated glycans in various tissues of mice, as detected ex vivo.[4] Similar to 9AzSia, Ac_4ManNAz administration failed to result in significant fluorescence of the tumors after in vivo reaction with DBCO–Cy5. The targeting effect of both azidosugars was negligible, as indicated by TBR values of 1.5 ± 0.2 (9AzSia) and 16.2 ± 2.8 (Ac_4ManNAz), and PNR values of 1.1 ± 0.1 (9AzSia) and 1.1 ± 0.1 (Ac_4ManNAz; Figure 2f). The low tumor targeting efficiency of Ac_4ManNAz is in agreement with previous reports by the Brindle group.[27,28] Taken together, our results indicate that the ligand-targeted liposomes not only achieve selectivity between positive and negative tumors, but also significantly improve the incorporation of the azides into the tumor-associated glycans. These two factors are probably both essential for realizing the targeted imaging of tumor-associated glycans in living mice.

The ability to achieve the targeted labeling and visualization of tumor-associated glycans in vivo should enable numerous studies of cancer glycobiology. One of the interesting applications is to monitor the dynamic changes of sialylation during tumor growth. To explore this, we performed in vivo targeted imaging of the newly synthesized sialylated glycans at different stages of tumor growth. The mice were implanted with B16–F10 tumors. After tumor growth for 7, 11, and 14 days, the mice were administered with cRGD–LP–9AzSia with the same dosages for another seven days, followed by injection with DBCO–Cy5 for in vivo imaging on day 14, 18, and 21, respectively. The fluorescence intensity of the tumors, which corresponds to the newly synthesized sialylated glycans, increased over time, indicating a time-dependent increase of biosynthesis of the sialylated glycans during tumor growth (Figure 3). It should be noted that the fluorescence intensity of whole-body images appeared dimmed in late-stage tumors, probably because those tumors grew deeper under the skin (Figure 3a). To better compare the relative fluorescence intensities at the three stages, the isolated tumors were imaged ex vivo (Figure 3b).

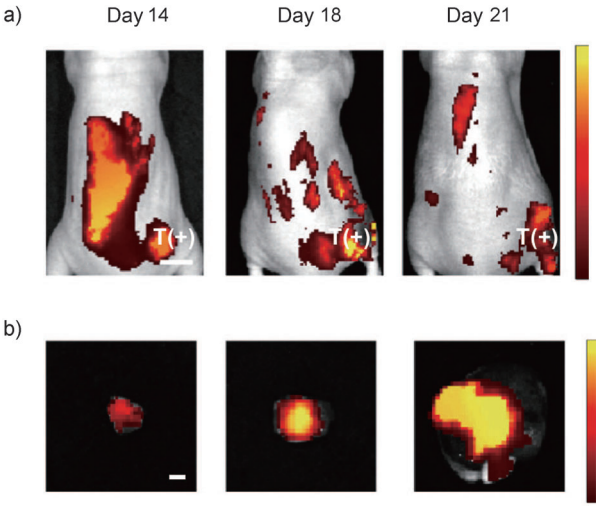

Figure 3. Monitoring the dynamic changes of sialylation during tumor growth. a) Representative in vivo fluorescence images of tumor-associated glycans in mouse models. Balb/c nude mice were xenografted with B16–F10 cells at the right dorsum. After tumor growth for 7, 11, and 14 days, cRGD–LP–9AzSia was injected into the mice for another 7 days, followed by injection with DBCO–Cy5. Five hours after the DBCO–Cy5 injection, the mice were directly visualized using an IVIS imaging system on day 14, 18, and 21, respectively. T(+) = integrin $\alpha_v\beta_3$-positive B16–F10 tumor. Scale bar: 1 cm. b) Ex vivo fluorescence images of isolated B16–F10 tumors at the corresponding stages. Scale bar: 0.2 cm. The color-coded scales represent the fluorescence intensity. Representative images from three experiments are shown.

Finally, we sought to enrich and identify the tumor-associated sialylated glycoproteins (Figure 4a). Notably, our method is well suited for investigating the newly synthesized glycoproteins during tumor growth owing to the metabolic incorporation of the azidosugars. B16–F10 tumor tissues labeled with cRGD–LP–9AzSia at the three stages were isolated from mice at day 14, 18, and 21, respectively, and the tissue lysates were reacted with alkyne-biotin, followed by enrichment with streptavidin beads. In-gel fluorescence analysis showed a decrease in labeling intensity for newly synthesized sialylated glycoproteins over time, suggesting a time-dependent decrease in the biosynthesis of sialylated glycoproteins (Figure 4b). Notably, the imaging results in Figure 3 indicate that the overall biosynthesis of sialome, which includes both glycoproteins and glycolipids, increases during tumor growth. These observations may be due to a strong increase in the biosynthesis of sialic acid-containing glycolipids.

We then subjected the enriched sialylated glycoproteins to gel-based proteomic identification by tandem mass spectrom-

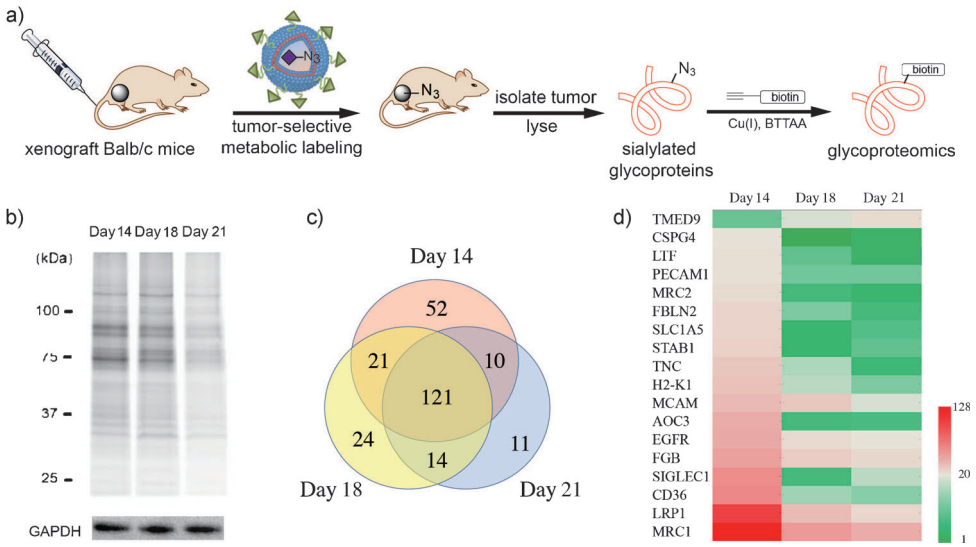

Figure 4. Proteomic analysis of sialylated glycoproteins associated with tumors. a) Experimental procedure for the selective enrichment and identification of sialylated proteins in tumor tissues. cRGD–LP–9AzSia is injected into the tumor-bearing mice. The azide-labeled tumors are then collected and homogenized, followed by reaction with biotin-alkyne by the copper-catalyzed click chemistry. Biotinylated glycoproteins are enriched by streptavidin beads and subjected to gel-based proteomic identification by tandem mass spectrometry. b) In-gel fluorescence scanning of tumor lysates. The mice were implanted with B16–F10 tumors for 7, 11, and 14 days, followed by a seven-day administration of cRGD–LP–9AzSia. Tumor lysates isolated on day 14, 18, and 21 were probed with Alexa Fluor 545 alkyne, resolved by SDS-PAGE, and the gel was directly scanned in a fluorescence imager. Anti-glyceraldehyde phosphate dehydrogenase (GAPDH) blot was used as the loading control. c) Overlap of identified sialylated proteins from three tumor growth stages for mice treated with cRGD–LP–9AzSia. d) Heat map of the spectral counts of representative proteins with significant changes in relative abundance. The color-coded scale represents the spectra counts.

etry. Using a high-confidence filter, that is, selecting only proteins with $\geq$5-fold increases of the spectra counts in the cRGD–LP–9AzSia treated samples above the cRGD–LP control samples, we selectively identified 204, 180, and 156 glycoproteins in day 14, 18, and 21 tumors, respectively (Tables S2–S4). Most of the identified proteins are membrane or secreted proteins with the consensus sequence of N-linked glycosylation (N–X–S/T, where X is any amino acid except proline). There are 121 sialylated glycoproteins commonly identified in all three stages (Figure 4c). Gene ontology analysis revealed several enriched biological processes, indicating that the tumor-associated sialylglycoproteins are mainly related to cell adhesion, wounding response, and inflammatory response (Figure S6). These processes have been proven to be important in tumor progression.[29,30] The relative abundances of the individual proteins identified in the three stages were compared according to their spectral counts (Figure S7).[31,32] Overall, most proteins showed lower spectral counts in later stages of tumor growth, which is in agreement with the in-gel fluorescence results. Those proteins with significant changes in abundance were selected for further analysis (Figure 4d). Considering the semi-quantitative nature of spectral counting, we set the selection criteria as follows: Only proteins with $\geq$20 spectral counts and $\geq$2-fold difference in the spectral counts between day 14 and day 21 samples were chosen. Several important cell-surface receptors, including the epidermal growth factor receptor (EGFR), sialic acid-binding immunoglobulin-like lectin 1 (SIGLEC1), and CD36, showed decreasing spectral counts. As only newly synthesized proteins into which the azidosugars had been metabolically incorporated were enriched and identified, these results suggest a decrease in the biosynthesis of these receptors or/and less sialylation on the newly synthesized receptors. Furthermore, we also identified a few proteins, such as transmembrane emp24 domain-containing protein 9 (TMED9), with increasing spectral counts.

In summary, we have demonstrated a strategy that makes use of ligand-targeted liposomes encapsulating azidosugars for the selective metabolic labeling of tumor-associated glycans with azides in living animals. The selectivity is achieved by the specific recognition of tumor-expressing receptors by the ligands on the liposome surface. In combination with click chemistry, liposomal azidosugars enable the in vivo fluorescence imaging of tumor-associated sialylated glycans and the proteomic identification of sialylated glycoproteins that are newly synthesized during tumor growth. Compared with labeling methods that use free azidosugars, our method offers improved labeling efficiency and high specificity. The facile procedure for preparing ligand-targeted liposomes allows for the introduction of various ligands for the targeting of different cancer types. Other azidosugars, such as *N*-azidoacetylgalactosamine[33] and azidofucose,[34] may also be explored for labeling different types of glycans. This work should facilitate the elucidation of the functional role of glycans in cancer biology.

Received: August 22, 2014
Published online: October 21, 2014

Keywords: click chemistry · integrin ligands · liposomes · sialic acids · tumor imaging

[1] R. Y. Tsien, *Angew. Chem. Int. Ed.* **2009**, *48*, 5612–5626; *Angew. Chem.* **2009**, *121*, 5721–5736.
[2] O. T. Keppler, R. Horstkorte, M. Pawlita, C. Schmidt, W. Reutter, *Glycobiology* **2001**, *11*, 11R–18R.
[3] S. T. Laughlin, C. R. Bertozzi, *Proc. Natl. Acad. Sci. USA* **2009**, *106*, 12–17.
[4] P. Carninci et al., *Nat. Genet.* **2006**, *38*, 626–635.

[5] R. M. Hoffman, M. Yang, *Nat. Protoc.* **2006**, *1*, 1429 – 1438.
[6] R. M. Hoffman, *Nat. Rev. Cancer* **2005**, *5*, 796 – 806.
[7] J. A. Prescher, D. H. Dube, C. R. Bertozzi, *Nature* **2004**, *430*, 873 – 877.
[8] D. H. Dube, J. A. Prescher, C. N. Quang, C. R. Bertozzi, *Proc. Natl. Acad. Sci. USA* **2006**, *103*, 4819 – 4824.
[9] D. H. Dube, C. R. Bertozzi, *Nat. Rev. Drug Discovery* **2005**, *4*, 477 – 488.
[10] M. M. Fuster, J. D. Esko, *Nat. Rev. Cancer* **2005**, *5*, 526 – 542.
[11] R. Xie, S. Hong, L. Feng, J. Rong, X. Chen, *J. Am. Chem. Soc.* **2012**, *134*, 9914 – 9917.
[12] P. Altevogt, M. Fogel, R. Cheingsong-Popov, J. Dennis, P. Robinson, V. Schirrmacher, *Cancer Res.* **1983**, *43*, 5138 – 5144.
[13] E. C. Seales, G. A. Jurado, B. A. Brunson, J. K. Wakefield, A. R. Frost, S. L. Bellis, *Cancer Res.* **2005**, *65*, 4645 – 4652.
[14] Y.-C. Liu et al., *Proc. Natl. Acad. Sci. USA* **2011**, *108*, 11332 – 11337.
[15] S. Julien et al., *Cancer Res.* **2011**, *71*, 7683 – 7693.
[16] T. Ju et al., *Cancer Res.* **2008**, *68*, 1636 – 1646.
[17] G. Yogeeswaran, P. L. Salk, *Science* **1981**, *212*, 1514 – 1516.
[18] A. Matsumoto, H. Cabral, N. Sato, K. Kataoka, Y. Miyahara, *Angew. Chem. Int. Ed.* **2010**, *49*, 5494 – 5497; *Angew. Chem.* **2010**, *122*, 5626 – 5629.
[19] P. M. van Hagen, W. A. Breeman, H. F. Bernard, M. Schaar, C. M. Mooij, A. Srinivasan, M. A. Schmidt, E. P. Krenning, M. de Jong, *Int. J. Cancer* **2000**, *90*, 186 – 198.
[20] M. Schottelius, B. Laufer, H. Kessler, H.-J. Wester, *Acc. Chem. Res.* **2009**, *42*, 969 – 980.
[21] A. Meyer, J. Auernheimer, A. Modlinger, H. Kessler, *Curr. Pharm. Des.* **2006**, *12*, 2723 – 2747.
[22] G. Bendas, L. Borsig, *Int. J. Cell Biol.* **2012**, *2012*, 676731.
[23] N. J. Agard, J. A. Prescher, C. R. Bertozzi, *J. Am. Chem. Soc.* **2004**, *126*, 15046 – 15047.
[24] M. F. Debets, S. S. van Berkel, S. Schoffelen, F. P. J. T. Rutjes, J. C. M. van Hest, F. L. van Delft, *Chem. Commun.* **2010**, *46*, 97 – 99.
[25] D. Peer, J. M. Karp, S. Hong, O. C. Farokhzad, R. Margalit, R. Langer, *Nat. Nanotechnol.* **2007**, *2*, 751 – 760.
[26] S. Lee et al., *ACS Nano* **2014**, *8*, 2048 – 2063.
[27] A. A. Neves, H. Stockmann, R. R. Harmston, H. J. Pryor, I. S. Alam, H. Ireland-Zecchini, D. Y. Lewis, S. K. Lyons, F. J. Leeper, K. M. Brindle, *FASEB J.* **2011**, *25*, 2528 – 2537.
[28] A. A. Neves, H. Stöckmann, Y. A. Wainman, J. C.-H. Kuo, S. Fawcett, F. J. Leeper, K. M. Brindle, *Bioconjugate Chem.* **2013**, *24*, 934 – 941.
[29] U. Cavallaro, G. Christofori, *Nat. Rev. Cancer* **2004**, *4*, 118 – 132.
[30] A. Mantovani, P. Allavena, A. Sica, F. Balkwill, *Nature* **2008**, *454*, 436 – 444.
[31] H. Liu, R. G. Sadygov, J. R. Yates, *Anal. Chem.* **2004**, *76*, 4193 – 4201.
[32] M.-Q. Dong, J. D. Venable, N. Au, T. Xu, S. K. Park, D. Cociorva, J. R. Johnson, A. Dillin, J. R. Yates, *Science* **2007**, *317*, 660 – 663.
[33] H. C. Hang, C. Yu, D. L. Kato, C. R. Bertozzi, *Proc. Natl. Acad. Sci. USA* **2003**, *100*, 14846 – 14851.
[34] M. Sawa, T.-L. Hsu, T. Itoh, M. Sugiyama, S. R. Hanson, P. K. Vogt, C.-H. Wong, *Proc. Natl. Acad. Sci. USA* **2006**, *103*, 12371 – 12376.